

## Hydrological simulation evaluation with WRF-Hydro in a large and highly complicated watershed: The Xijiang River basin

Songnan Liu <sup>a,c</sup>, Jun Wang <sup>a,b,\*</sup>, Jiangfeng Wei <sup>a,c</sup>, Huijun Wang <sup>a,b,c</sup>

<sup>a</sup> Collaborative Innovation Center on Forecast and Evaluation of Meteorological Disasters, Ministry of Education, Nanjing University of Information Science and Technology, Nanjing 210044, Jiangsu, China

<sup>b</sup> Nansen-Zhu International Research Centre, Institute of Atmospheric Physics, Chinese Academy of Sciences, Beijing 100029, China

<sup>c</sup> Key Laboratory of Meteorological Disaster, Ministry of Education, Nanjing University of Information Science and Technology, Nanjing 210044, Jiangsu, China



### ARTICLE INFO

**Keywords:**

WRF-Hydro  
Streamflow  
Application  
Soil moisture  
Evapotranspiration  
IHA

### ABSTRACT

**Study region:** Xijiang River, South China.

**Study focus:** This paper discusses the application of WRF-Hydro, a distributed hydrological model, to a complicated watershed. The model performance on simulating streamflow, soil moisture, soil temperature and evapotranspiration is evaluated. Changes and characteristics of streamflow and related variables simulated by the model are analyzed.

**New hydrological insights for the region:** In this study, thirteen sensitive parameters used in this model are tested in large and small watersheds of the basin. It is found that large basins are more sensitive to base flow parameters than small basins. The WRF default soil type dataset is replaced by the Beijing Normal University (BNU) soil type dataset that is more accurate. The model can simulate temporal changes of streamflow as well as temporary variabilities of hydrological variables. The model can be applied in small and large watersheds. The trend of streamflow in the basin is spatially uneven with an increasing trend in the upper part and a decreasing trend in the lower part. The changes in streamflow are partly related to precipitation and evapotranspiration trends. The trends of 30-day maximum/minimum streamflow are not significant, but the reversals demonstrate significant changes during 1980–2018. This study is expected to serve as a reference for the application of the model in this basin and model calibration over different sizes of study area.

### 1. Introduction

Knowledge of hydrological cycle is important for water resources management and assessment of water-related hazards such as floods and droughts (Liu et al., 2008; Wang et al., 2011). In the context of global warming, the magnitude and frequency of hydrological disasters are increasing (Ma et al., 2019; Winsemius et al., 2016).

Hydrological models are the most important tool for the simulation and forecast of hydrological processes. These models can be used to predict floods and droughts, and help water resources management (Beskow et al., 2011). Hydrological models can be roughly divided into two types: lumped models and distributed models (Devia et al., 2015). In lumped models, the spatial variability is

\* Corresponding author at: Nansen-Zhu International Research Centre, Institute of Atmospheric Physics, Chinese Academy of Sciences, Beijing 100029, China.

E-mail address: [wangjun@mail.iap.ac.cn](mailto:wangjun@mail.iap.ac.cn) (J. Wang).

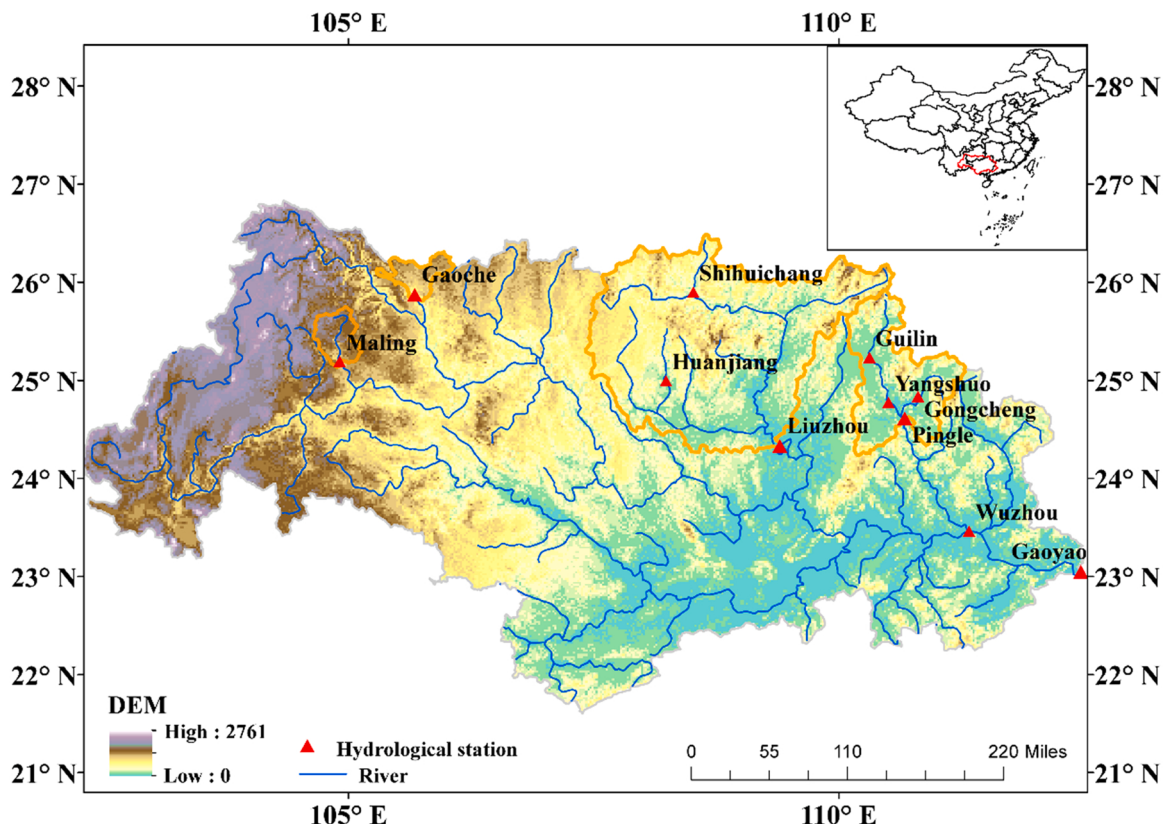


**Fig. 1.** Topography and distribution of hydrological stations (red triangles), the sub-basins (orange lines), and the river (blue line) above the Gaoyao station in the Xijiang River basin. (For interpretation of the references to color in this figure legend, the reader is referred to the web version of this article.)

neglected, and the entire river basin is taken as one unit. Therefore, the spatial processes in the watershed are not explicitly considered. Different to lumped models, the spatial variations of parameters, variables and conventional hydrometeorological data are considered in distributed models. The entire watershed is divided into small units to produce predictions in distributed models. Therefore, the intra-basin variability can be carefully studied, and the values of model parameters from geospatial data (such as land cover and soil types) can be inferred (Wang et al., 2011). With the development of the geographic information system and computer sciences, distributed models have been improved and widely used in recent years (Lei et al., 2014).

In this paper, a distributed hydrological model, i.e., the Weather Research and Forecasting Model Hydrological modeling system (WRF-Hydro v5.0) (Gochis et al., 2018) is evaluated in the Xijiang River basin. WRF-Hydro is interactively coupled with the NOAH land surface model (LSM), which includes kinetic and thermal processes (Gochis et al., 2018; Senatore et al., 2015). WRF-Hydro can be used as an offline hydrological model, while it can also be coupled with atmospheric models (e.g. Weather Research and Forecasting Model, WRF) and other earth system modeling systems to form a coupled architecture. The model can simulate and predict hydrological processes at various spatial scales (from headwater catchment to continental river basin) and temporal resolutions (from minute to season). It can be run efficiently on high-performance computing systems. WRF-Hydro provides the ArcGIS Tools (Gochis et al., 2018) to generate the model static inputs, which are important for its applications. The model has been used in a wide range of researches and applications, including flash flood prediction (Lin et al., 2018; Varlas et al., 2019), seasonal forecast of water resources (Kerandi et al., 2017; Somos-Valenzuela and Palmer, 2018) and land-atmosphere-sea coupling studies (Rummel et al., 2019; Varlas et al., 2018). Senatore et al. (2015) indicated that WRF-Hydro can rightly simulate the land surface water cycle processes with a 3-year simulation in southern Italy. Arnault et al. (2016) proposed that WRF-Hydro can reflect the impact of land-atmosphere processes on surface runoff. Kerandi et al. (2017) found that WRF-Hydro coupled with WRF (Weather Research and Forecasting Model) model can be used as a tool to quantify the atmospheric-terrestrial water balance in the Tana River basin. Ryu et al. (2017) revealed that WRF-Hydro coupled with WRF model can help predict flood events in a small watershed in Korea. Silver et al. (2017) pointed out that WRF-Hydro coupled with WRF model can truly reflect the actual runoff changes in the arid/semi-arid of Israel and Jordan. Despite its wide application around the world, WRF-Hydro is rarely used in China and its performance in China, especially in large scale basins with complicated terrain, should be carefully examined.

The Xijiang River (West River) is the longest river in the basin of the Pearl River. It provides 63.9% of the total river discharge and accounts for 77.8% of the total area of the Pearl River (Zhong et al., 2018), which makes it very important for the socio-economic

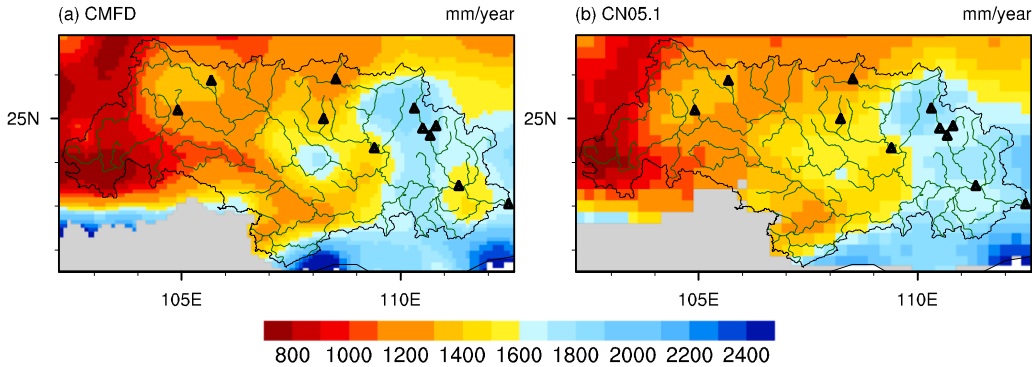


**Fig. 2.** Annual mean precipitation (units: mm/year) during 1980–1984 and 2006–2014, where (a) is the CMFD precipitation and (b) is the CN05.1 precipitation. The black triangles denote hydrological stations. (For interpretation of the references to color in this figure legend, the reader is referred to the web version of this article.)

development in South China (Yuan et al., 2017). Because of its importance for the Pearl River Delta, the Xijiang River is also called the Golden Waterway (Lin et al., 2017). The water resource in the Xijiang River basin is an important component of the water supply that meets the demand of the Pearl River Delta (Sun and Niu, 2019). Besides, both floods and droughts occur frequently in the Xijiang River basin (Cui et al., 2007). In recent years, this basin has experienced more floods and droughts (Yuan et al., 2017) due to the influence of global warming. The geological environment of the Xijiang River basin is very complicated, which leads to complex land surface processes and hydrological processes. Thereby, hydrological simulation and forecast in this basin remains an extremely challenging issue. A hydrological model with complete dynamic and thermal processes is required for realistic simulation and prediction of hydrological conditions in this basin. WRF-Hydro is a good choice to serve these requirements. Some hydrological models have been applied to this basin, but the resolutions of those models are relatively coarse (Chen et al., 2019; Jiang et al., 2011; Shan et al., 2015; Yuan et al., 2014). In this study, WRF-Hydro model is applied to the Xijiang River basin for processes studies over both small sub-basins and the entire river basin with a relatively high spatial resolution. The object of this study is to evaluate the performance of WRF-Hydro in reproducing the streamflow and hydrological conditions in the Xijiang River mainstream basin and its several sub-basins, and determine whether the model is suitable for studies over both large and small basins with different topographies. Also, the changes and characteristics of the streamflow during 1980–2018 and their possible causes are explored and discussed.

## 2. Data and method

### 2.1. Study area

The Pearl River is the second-largest river in China in terms of annual streamflow, and the Xijiang River is the largest tributary of the Pearl River (Yuan et al., 2017). The Xijiang River originates in the east of the Maxiong Mountain, flows through Yunnan, Guizhou, Guangxi and Guangdong provinces, and ultimately flows into the South Sea. The length of the Xijiang River is 2214 km and the drainage area is 346,000 km<sup>2</sup>, which accounts for nearly 80% of the total drainage area of the Pearl River basin (Niu et al., 2015). It is important for the development of the economy and culture in Guangdong province and Guangxi province. This area is characterized by complex terrain with several land use types (Fig. 3) and various climate regimes. The west part, representing the upstream of the river, is mainly a mountainous area; the east, representing the downstream of the river, is flat. The topography and the location of the Xijiang River basin are shown in Fig. 1.

The Xijiang River basin is located in a tropical and subtropical region that is hot and humid. The annual average temperature is around 20 °C; the annual average air humidity is about 75%; the annual average rainfall approximately is 1700 mm. The spatial distribution of annual mean rainfall (1980–1984 and 2006–2014) is shown in Fig. 2. Due to the monsoon rainfall, both precipitation and streamflow demonstrate large seasonal variabilities (Zhang et al., 2009). This river is a semi-perennial river, whose streamflow is low in dry season but increases significantly in wet season. The precipitation from April to September accounts for nearly 65% of the annual mean precipitation, and the streamflow from April to September accounts for nearly 75% of the annual mean streamflow (Yu et al., 2016).

In order to study the model's applications in different conditions of terrain and land use, several tributaries of the Xijiang River are selected, including the Beipanjiang River (Gaoche station is the representative station) and the Mabie River (Maling station is the representative station) in the upstream of the Xijiang River, and the Liujiang River (Liuzhou station is the representative station) and the Guijiang River (Pingle station is the representative station) in the downstream of the Xijiang River (shown in Fig. 1). The elevations of the Beipanjiang River and the Mabie River basins are higher compared with the elevations of the Liujiang River and the Guijiang River basins. The predominant landuse type is savannas in the Beipanjiang River, the Mabie River basin and the Guijiang River basins. Woody savannas is the prevailing landuse type in the Liujiang River basin (shown in Fig. 3).

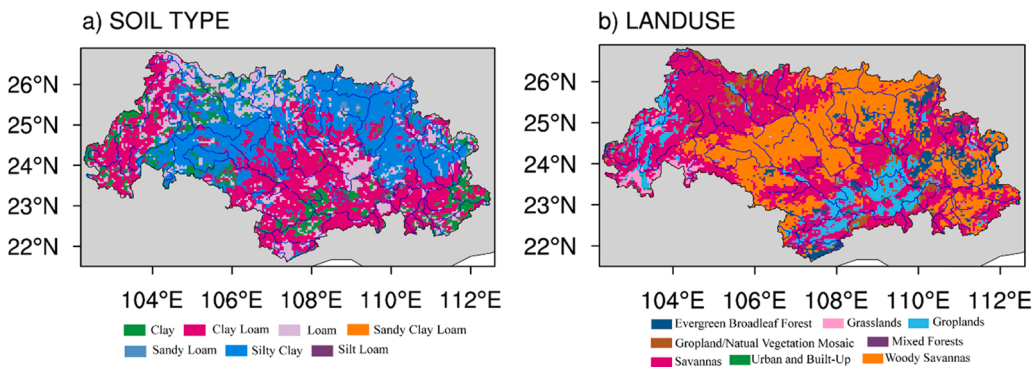


**Fig. 3.** Spatial distributions of soil and landuse types in the Xijiang River basin.

## 2.2. Datasets

WRF-Hydro requires a number of files to describe the model domain, parameters, initial condition and meteorological conditions. The high-resolution global DEM data are extracted from the HydroSHEDS data (Hydrological data and maps based on SHuttle Elevation Derivatives at multiple Scales, <https://hydrosheds.cr.usgs.gov/dataavail.php>). The HydroSHEDS DEM dataset is developed based on high-resolution Radar Topography Mission (SRTM). The resolution of this dataset is divided into three categories, that is 3" (about 90 m), 15" (about 500 m) and 30" (about 1 km) (Lehner et al., 2008). Due to the area size and complexity of the Xijiang River basin, the resolution of 15" is selected for this research. The DEM is processed by ArcGIS to get the accurate river network.

To run the offline model, several meteorological variables are needed. These variables include downward long-wave radiation, downward short-wave radiation, surface pressure, precipitation rate, specific humidity, air temperature, near surface U and V wind components. The main source of meteorological data used in this paper is the China Meteorological Forcing Dataset (CMFD), which is a near-surface meteorological reanalysis dataset developed by the Institute of Tibetan Plateau Research of the Chinese Academy of Sciences. This dataset is developed based on the Princeton reanalysis data, GLDAS (Global Land Data Assimilation System) data, GEWEX-SRB (Global Energy and Water cycle Experiment-Surface Radiation Budget) radiation data, TRMM (Tropical Rainfall Measuring Mission) precipitation data, and conventional meteorological observation data of China Meteorological Administration. Its temporal resolution is 3 h and its spatial resolution is 0.1° (Chen et al., 2011). This dataset has been used in the fields of hydrology, climate simulation and land surface process simulation (Ma et al., 2019; Sun et al., 2017). Since CMFD only includes wind speed but no wind direction, which is required by WRF-Hydro, U and V wind components of ERA5 are also used in this research. The ERA5 (Hersbach et al., 2020) is a reanalysis dataset released by the European Center for Medium Range Weather Forecasts with horizontal resolution of 30 km, and the ERA5 data at 6-hour intervals are used in our research.

Precipitation plays an important role in hydrological models (Liu et al., 2017). CN05.1 is a widely used daily precipitation dataset with a resolution of 0.25°, and it is based on in-situ observations at over 2400 weather stations in China (Wu and Gao, 2013). The resolution of CN05.1 is coarse compared with the model resolution (5000 m and 6 h) and cannot meet the research demand. Therefore, the precipitation of CMFD is used. The precipitation of CMFD was evaluated before it is implemented for the present study. Distributions of annual mean precipitation over the basin during the periods of 1980–1984 and 2006–2014 derived from the CN05.1 and CMFD are compared (Fig. 2). It can be seen that the annual mean precipitation decreases from southeast to northwest for both datasets. The spatial correlation coefficient and the root-mean-square-error (RMSE) between CMFD and CN05.1 precipitation are 0.84 and 3.1 mm, respectively. The performance of the CMFD precipitation dataset is acceptable, and thus this dataset is used in the present research.

The observed streamflow data are extracted from the published Hydrological Yearbook. The books are borrowed from the library of the Hohai University. Due to the incompleteness of the dataset, the time period is divided into two parts, 1980–1984 and 2006–2014. 1979 and 2005 (running ten times) are used to spin-up the model, separately. The model is calibrated over the period 2006–2010, while the two periods 1980–1984 and 2011–2014 are used for the verification of the model.

To evaluate the simulated soil moisture, soil temperature and evapotranspiration, the soil moisture and soil temperature of CLDAS (China Meteorological Administration Land Surface Data Assimilation System Real-Time Product Dataset), the observed monthly soil moisture (observation stations) and observed daily evaporation (observation stations in China) are used. CLDAS is developed by the National Meteorological Information Center of China, which has a temporal resolution of 1 h and a spatial resolution of 1/16° × 1/16° (Han et al., 2015). The dataset starts from 2008. The soil moisture of the dataset has a good agreement with the ground soil moisture observations with an average correlation coefficient of 0.89 and a RMSE of 0.02 m<sup>3</sup>/m<sup>3</sup> in China. The soil temperature of the dataset also agrees well with the ground soil temperature observations with a correlation coefficient of 0.99 and a RMSE of 1.22 K in China.

## 2.3. Statistical methods

The performance of WRF-Hydro in simulating streamflow is quantitatively evaluated through several typical statistical metrics including correlation coefficient (CC), Nash efficiency coefficient (NSE), logarithmic efficiency score (NSE(logQ)), RMSE and relative

**Table 1**

The details of IHA parameters.

IHA Groups	Hydrological parameters			
Group 1	Mean value in January	Mean value in February	Mean value in March	Mean value in June
	Mean value in April	Mean value in May	Mean value in September	Mean value in December
	Mean value in July	Mean value in August	Annual minima, 1-day means	Annual maxima, 1-day mean
	Mean value in October	Mean value in November	Annual minima, 3-day means	Annual maxima, 7-day means
Group 2	Annual minima, 30-day means	Annual minima, 90-day means	Annual maxima, 7-day means	Annual maxima, 7-day means
	Annual maxima, 3-day means	Number of zero-flow days	Base flow index	
	Annual maxima, 7-day means	Date of minimum		
	Date of maximum	High pulse count		
Group 3	High pulse duration	Low pulse count		
	Low pulse duration	Rise rate	Fall rate	Number of reversals
Group 5				

error (*Bias*, units: %). They are defined by Eqs. (1), (2), (3), (4) and (5), respectively. Though these metrics are mathematically related, each of them has certain differences from others. Together they could lead to a more comprehensive understanding of the performance of the model (Tedeschi, 2006). *CC* reflects the linear relationship between simulations and observations. It ranges from -1.0 to 1.0, and a value of 1 represents perfect positive correlation performance. *NSE* is a commonly used metric in hydrological evaluations, which measures both the magnitude of errors and the variability of timeseries. It ranges from minus infinity to 1.0 (Nash and Sutcliffe, 1970), and the ideal value is 1. The closer the value is to 1, the better the model performance. If the value is 0, the model performance is just as good as yielding the mean observation. If the value is less than 0, the performance of the model is poor. *NSE(logQ)* is used to test the model performance in simulating streamflow during the low-flow period in winter (Beskow et al., 2011). Its value is within the range from  $-\infty$  to 1, and the ideal value is 1. *RMSE* is used to measure the deviation between simulations and observations, with a range from 0 to  $\infty$ , and the ideal value is 0. *Bias* reflects the range of underestimation or overestimation, and the ideal value is 0.

$$CC = [n \sum (Q_{obs,i} Q_{mod,i}) - \sum Q_{obs,i} \sum Q_{mod,i}] / \{[n \sum Q_{obs,i}^2 - (\sum Q_{obs,i})^2]^{1/2} [n \sum Q_{mod,i}^2 - (\sum Q_{mod,i})^2]^{1/2}\} \quad (1)$$

$$NSE = 1 - \sum (Q_{obs,i} - Q_{mod,i})^2 / \sum (Q_{obs,i} - Q_{obs,i}^*)^2 \quad (2)$$

$$NSE(\log Q) = 1 - \sum [\log(Q_{obs,i}) - \log(Q_{mod,i})]^2 / \sum [\log(Q_{obs,i}) - \log(Q_{obs,i}^*)]^2 \quad (3)$$

$$RMSE = [\sum (Q_{obs,i} - Q_{mod,i})^2 / n]^{1/2} \quad (4)$$

$$Bias = (Q_{mod,i} - Q_{obs,i}) / \sum Q_{obs,i} \times 100\% \quad (5)$$

Where  $Q_{obs,i}$  denotes the i-th observed streamflow,  $Q_{mod,i}$  denotes the i-th model simulated streamflow,  $Q_{obs,i}^*$  denotes the temporal average of observed streamflow,  $n$  is the number of days.

To describe the change of streamflow, several statistical metrics are used, including linear regression, 5-year running average, and indicators of hydrologic alteration (IHA). IHA is one of the popular metrics, which is proposed to describe the characteristics and variation of streamflow. The IHA contains 33 hydro statistical metrics, which can be divided into the following 5 groups: magnitude of monthly streamflow condition, magnitude and duration of annual extreme streamflow condition, timing of annual extreme water condition, frequency and duration of high and low pulses, and rate and frequency of water condition change. The details of these parameters are shown in Table 1. Group 1 is used to show the characters and trends of streamflow in different months. Group 2 is used to evaluate the peculiarity of annual minimum and maximum streamflow, and the base flow index is presented by the ratio of the 7-day minimum streamflow to the annual mean streamflow. Group 3 shows the date of maximum/minimum streamflow in every year. Group 4 shows the periods wherein daily streamflow exceeds the 75th percentile or drops below the 25th percentile of the time-series. Group 5 represents the streamflow reversals (from increasing to decreasing or from decreasing to increasing), which show the rate and frequency of the streamflow changes.

## 2.4. Models

WRF is used to provide the initial conditions (such as land use and soil type) for WRF-Hydro, and in this section the details of WRF are described. WRF is a mesoscale meteorological model developed by the National Centers for Environmental Prediction (NCEP) and the National Center for Atmospheric Research (NCAR) (Skamarock et al., 2008). There are two types of dynamic cores: ARW (Advanced Research WRF) and Non-hydrostatic Mesoscale Model (NMM), and the ARW dynamic core is used in this research. The land use and soil type are extracted from the MODIS (Moderate Resolution Imaging Spectroradiometer) land use dataset and Beijing Normal University Soil Type Dataset (Fig. 3), respectively.

WRF-Hydro is a distributed hydrological model that can be applied to the study of hydrometeorology and hydroclimatology. The model can be either used in an offline mode or in a coupled mode, in which it is coupled with atmospheric or earth system models. WRF-Hydro extends the traditional Noah land model by providing the framework of routing, including base flow process, subsurface flow process, surface overland flow process and channel routing. In this study, in addition to the surface process, the base flow process and subsurface flow process are also activated. WRF-Hydro v5.0 is used in this research. The resolutions of LSM grid and routing grid

**Table 2**

Calibrated parameters in this research.

Parameters	Units	Description	Main Hydrological response	Range
REFKDT	unitless	Parameter in surface runoff	Partitioning of total runoff into surface and subsurface runoff	0.1–5
LKSATFAC	unitless	Multiplier on Saturated soil lateral conductivity	Routing/Interflow process	10–10,000
RETDEPRTFAC	unitless	Maximum retention depth	Routing/Interflow process	0.1–10
SLOPE	unitless	Slope index	Aquifer recharge	0.1–1
OVROUGHRTFAC	unitless	Roughness scaling parameter	Routing/Interflow process	0–1
Manning	unitless	Manning's roughness coefficient	Routing/Interflow process	depend on the channel order
Expon	unitless	Parameters of the GW model	Baseflow	
Zmax	mm			
C	$m^3/s$			
SMCMAX	$m^3/m^3$	Saturated soil moisture	Infiltration	depend on soil type
DKSAT	$m/s$	Saturated soil hydraulic conductivity	Infiltration	depend on soil type

can be different, which allows a higher resolution for the process of routing. For each timestep the meteorological forcing is available, a sub-grid spatial-weighting method is used to disaggregate from LSM grid to routing grid. In this study, the LSM resolution is 5000 m, and the routing resolution is 500 m.

## 2.5. Model calibration

Due to the uncertainties of parameters, parameters calibration is crucial for WRF-Hydro model. In this section, the influences of parameters on the streamflow are evaluated. The model spin-up time is 10 years. The model is calibrated against the observed streamflow at each sub-basin and the main basin during 2006–2010. The validation is done against several datasets, including the observed streamflow at the outlet during 2011–2014 and observed streamflow at the interior stream stations during 2011–2014. Since the automatic calibration requires large computation time to optimize parameters, manual calibration is performed in this study. [Yucel et al. \(2015\)](#) proposed four parameters that are important for streamflow simulation, i.e., the runoff infiltration parameter (REFKDT) that is used to divide the total water into surface runoff and under-surface runoff, the surface retention depth scaling parameter (RETDEPRTFAC) that can adjust the initial retention depth, the overland flow roughness scaling parameter (OVROUGHRTFAC) that controls the speed of infiltration excess water that flows into channel networks, and the channel Manning roughness (MannN) that is related to the channel roughness. According to [Naabil et al. \(2017\)](#), lateral saturated conductivity scaling factor (LKSATFAC) and slope index (SLOPE) are also related to the runoff simulation. The spatial distribution of soil hydraulic properties can influence the performance of WRF-Hydro. Therefore, saturated soil moisture (SMCMAX) and saturated soil hydraulic conductivity (DKSAT) that influence flood generation mechanisms are considered in this research. Besides, the parameters related to base flow are considered. The calibration approach is divided into two parts. The parameters related to water volume are calibrated first, including the summer peaks (REFKDT) and base flow (SLOPE, BEXP, C, and Zmax), and the parameters related to hydrograph shapes (OVROUGHRTFAC, LKSATFAC, RETDEPRTFAC and MannN) are then calibrated ([Yucel et al., 2015](#)). If the values of the above parameters are constant in the basin, the values will be replaced by the calibrated values; if the values are spatially varying, then multipliers are applied to the initial values. The details of those calibrated parameters are shown in [Table 2](#). The influence of base flow is small for the three sub-basins, but its influence for the main basin is large.

## 3. Results

The model performance is evaluated in two forms: streamflow hydrographs at selected stations and spatial distribution of hydrological variables. The linear regression analysis and 5-year running average are applied to reveal changes in the hydrological characteristics.

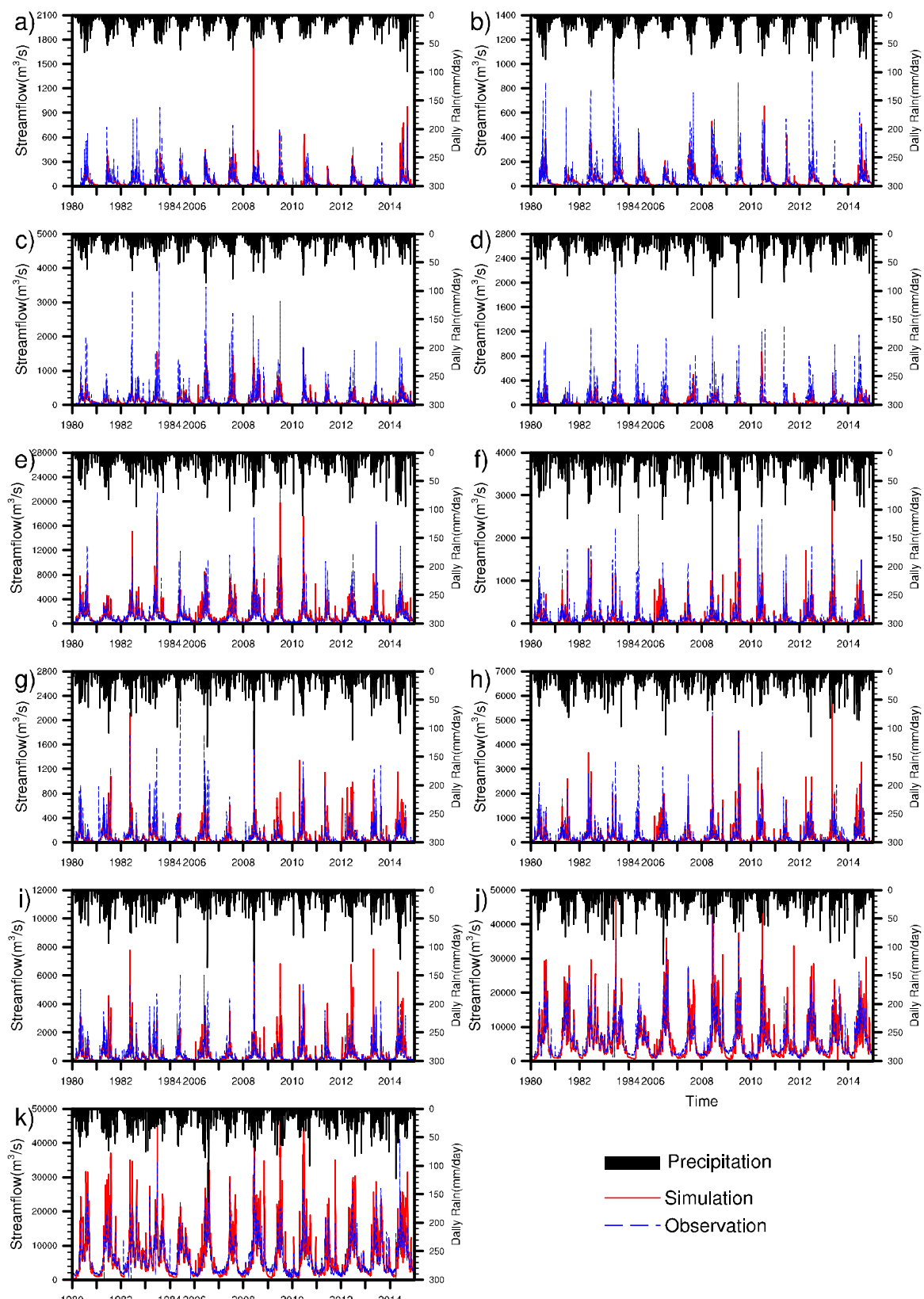
### 3.1. Model performance

#### 3.1.1. Streamflow

To evaluate the model performance on simulating streamflow, the Xijiang River basin and its three sub-basins with 11 hydrological stations (shown in [Fig. 1](#)) are selected. The spatial distribution of these stations makes a relatively full coverage of the Xijiang River basin.

[Fig. 4](#) shows daily streamflow at 11 stations during the calibration period and the two verification periods. The model performance on daily streamflow simulation is good at most stations with high CCs and reasonable NSEs and low Biases. However, the model underestimates streamflow at the upper part of the Xijiang River basin and at some small sub-watersheds, whereas it overestimates streamflow at the lower part of the Xijiang River basin and some large sub-watersheds.

From the hydrographs of the Maling station (located in the Mabie River basin) and Gaoche station (located in the Beipanjiang River basin), it can be seen that the simulated streamflow is lower than the observed streamflow in both wet and dry periods. But the model



Precipitation  
Simulation  
Observation

(caption on next page)

**Fig. 4.** Hydrographs of simulated streamflow (red line) and observed streamflow (blue dashed line) at 11 stations for one calibration period and two verification periods: a) Maling, b) Gaoche, c) Shihuichang, d) Huangjiang, e) Liuzhou, f) Guilin, g) Gongcheng, h) Yangshuo, i) Pingle, j) Wuzhou, k) Gaoyao. (For interpretation of the references to color in this figure legend, the reader is referred to the web version of this article.)

realistically reproduces temporal variation of the streamflow. The hydrograph of the Liuzhou station (located at the outlet of the Liujiang River) indicates that the simulated streamflow well matches the observed streamflow in both the magnitude and the timing. The performance of simulating peak streamflow is good, with the *NSE* is 0.82 for simulated streamflow, higher than 75% of the observed streamflow in the calibration period. However, the model underestimates streamflow at the tributaries of the Liujiang River (Fig. 4(c) and (d)). The hydrograph of the Pingle station (located at the outlet of the Guijiang River) shows that WRF-Hydro underestimates the streamflow during 1980–1984 and overestimates it during 2011–2014. But the model performs well in simulating the timing of the streamflow, and in the calibration period the *NSE* is 0.75 for simulated streamflow, higher than 75% of the observed streamflow. From the hydrographs of the Wuzhou station and Gaoyao station (located in the lower reaches of the Xijiang River), it can be seen that the model overestimates the streamflow in flood periods, but the simulated timing is basically correct.

Table 3 gives the results of the statistical metrics for all stations. These results indicate that the model performance on streamflow simulation is worse during 2011–2014 than during 1980–1984, which reflects the fact that when the model simulation is not realistic, often the same unrealistic result can be found for the whole basin (Motovilov et al., 1999). WRF-Hydro underestimates streamflow in most sub-basins, whereas it overestimates the streamflow in the main river basin. The correlation coefficients for all stations are above 0.5 and can reach up to 0.95 at some stations. This result suggests that the model can properly simulate the temporal variability of streamflow. The values of *NSEs* are above 0.3 for most stations and above 0.75 for some stations. The *Biases* are negative for most stations, but in the lower reaches of the Xijiang River mainstream and the outlets of the sub-basins, the *Biases* are positive. Note that the value of *NSE(log(Q))* is highly influenced by the recession period of the hydrograph. While the values of *NSE(log(Q))* are slightly lower than *NSE*, they are acceptable for most stations. This result indicates that the model has the ability to capture the streamflow during dry periods. Gaoche, Liuzhou, Pingle and Gaoyao stations are selected to calibrate the model for each basin. Therefore, the model performance in those stations are better compared with the un-calibrated stations in each basin. Huanjiang and Shihuichang stations are located at the tributaries of the Liujiang River, and Liuzhou station was used to calibrate the model in the Liujiang River. Therefore, the parameters may not be suitable for these two stations. For Gaoche and Maling stations, there are reservoirs in the upstream of the basin, and the human activities may influence the model performance. Besides, those two basins are small and the China Meteorological Administration stations CMFD used are sparse in those basins, the accuracy of the CMFD may also influence the performance.

Based on the hydrographs and statistical metrics results for all stations, it can be found that WRF-Hydro can simulate temporal variability of daily streamflow for all the stations. The model can simulate streamflow over different terrain areas from mountains (the upper reaches of the Xijiang River) to plains (the lower reaches of the Xijiang River).

The scatterplots of simulated and observed monthly streamflow are shown in Fig. 5. The orange and purple lines are the linear regression lines for the periods 1980–1984 and 2011–2014, respectively. And the black line is a 45-degree line.  $R^2$  is the coefficient of determination, and a higher  $R^2$  means a better linear relationship between simulations and observations. The scatters for most stations are evenly distributed along the black line, indicating that the model can well simulate the seasonal variation of streamflow. At the Maling station, the model overestimates streamflow for the period 1980–1984 but underestimates it for the period 2011–2014. At Gaoche station, the orange and purple lines are below the black line, which means that the model underestimates the streamflow in most months. The model underestimates streamflow in almost every month at Shihuichang and Huanjiang stations. At Liuzhou, Guilin, Yangshuo and Pingle stations, the model performance on the simulation of streamflow magnitude is good, and the  $R^2$  corresponding to the orange and purple lines are larger than 0.72. This result indicates that the model performs well in simulating temporal changes of streamflow at these stations. The model overestimates streamflow for the period 2011–2014 and underestimates it for period 1980–1984 at Gongcheng station. At Wuzhou and Gaoyao stations, the model slightly overestimates the streamflow and the  $R^2$  are high, which means that the model performance on the simulation of temporal variation of streamflow is good. As for the monthly streamflow simulation, the *CCs* are higher than 0.9 for most stations, and the *NSEs* reach 0.85 for some stations. The model simulation of monthly streamflow is evaluated to be ‘good’ when  $NSE > 0.65$  and  $-25\% < Bias < 25\%$ , and ‘very good’ when  $NSE > 0.75$  and  $-10\% < Bias < 10\%$  (Moriasi et al., 2007). Based on the metrics listed in Table 4, it is found that the model performance can be regarded as ‘very good’ for several stations and “good” for most stations. Overall, the model performance on monthly streamflow simulation is satisfactory, and the model demonstrates the ability to simulate the seasonal variations of streamflow.

### 3.1.2. Soil conditions

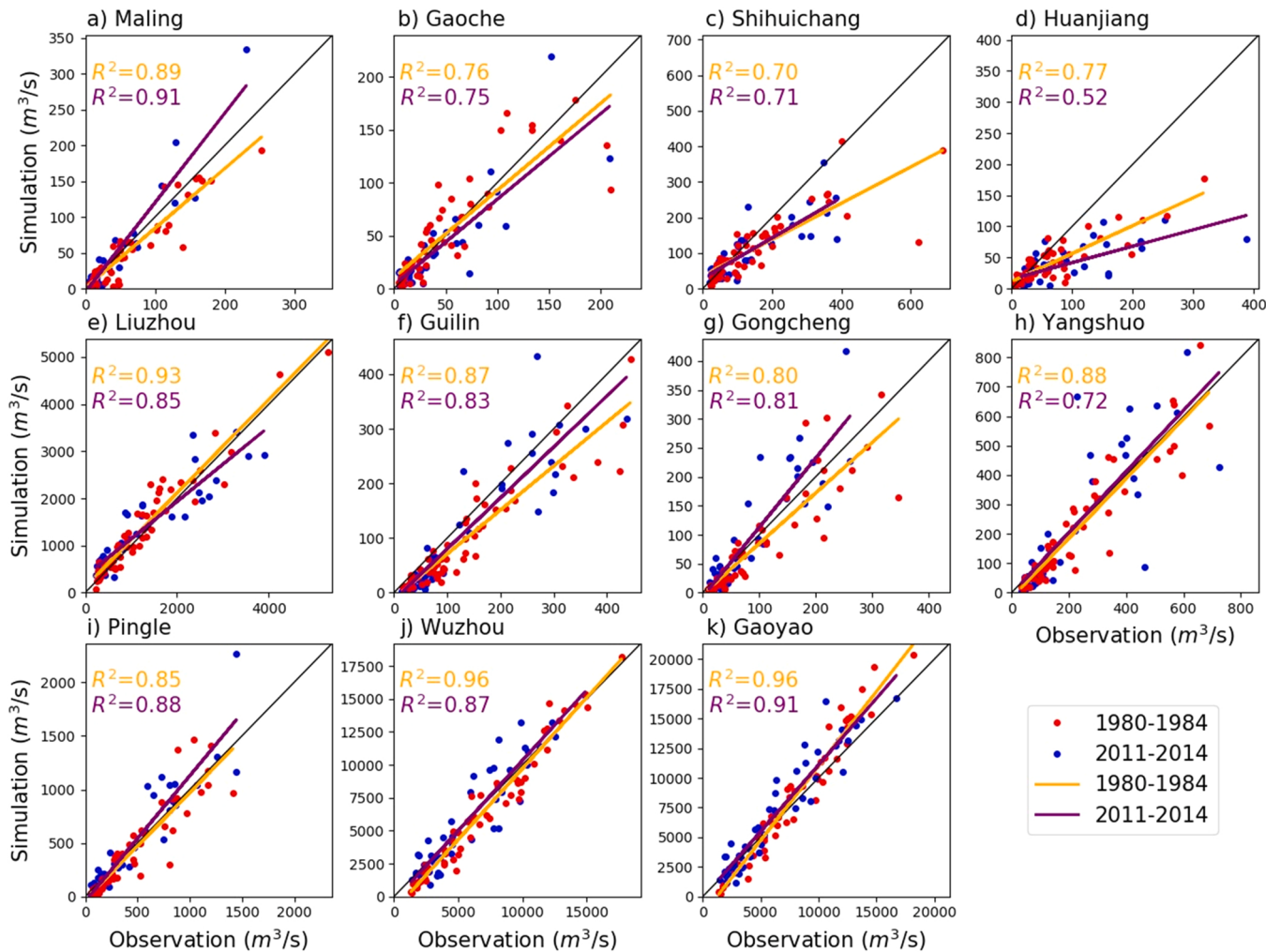
Soil moisture is an important variable that measures the dry and wet conditions of soil (Legates et al., 2011), and there are complicated interactions between soil moisture and climate elements (Tuttle and Salvucci, 2016; Walker and Rowntree, 1977; Wei et al., 2008). Researchers have found that soil moisture is an influential factor for climate anomalies (Stéfanon et al., 2013; Wei and Dirmeyer, 2012). Due to the memory of soil moisture, it can help predict future weather and climate (Douville and Chauvin, 2000; Guo and Dirmeyer, 2006). Soil temperature is a measurement of soil heat storage. It is an important physical property of soil and has significant climatic effects (Carson and Moses, 1963; Bai et al., 2010; Xue et al., 2012).

Fig. 6 shows the *CCs*, *Biases* and *RMSEs* of monthly soil moisture between simulations and station observations during 1992–2013. It can be seen that the model can capture the temporal variability of the soil moisture with the *CCs* larger than 0.7 at the upper part of the Xijiang River and some areas of the lower part. Fig. 6(b) shows that the model overestimates soil moisture for most areas. The *RMSEs* are lower than  $0.13 \text{ m}^3/\text{m}^3$  at all stations, and the average *RMSE* is about  $0.07 \text{ m}^3/\text{m}^3$ , which is within the acceptable range.

**Table 3**

Quantitative analysis results of model performance on daily streamflow simulation.

STATION	CC			NSE			NSE (logQ)			Bias (%)			RMSE ( $\text{m}^3/\text{s}$ )		
	Time	2006–2010	1980–1984	2011–2014	2006–2010	1980–1984	2011–2014	2006–2010	1980–1984	2011–2014	2006–2010	1980–1984	2011–2014	2006–2010	1980–1984
Maling	0.68	0.68	0.86	0.16	0.45	0.63	0.23	0.51	0.54	10.12	-15.06	10.19	66.85	62.42	40.13
Gaoche	0.64	0.63	0.61	0.3	0.4	0.35	0.43	0.61	0.57	1.25	4.66	-8.9	58.64	64.09	51.28
Shihuichang	0.78	0.61	0.74	0.58	0.33	0.48	0.67	0.60	0.58	-15.58	-23.1	-17.03	170.69	193.24	123.39
Huanjiang	0.54	0.74	0.55	0.2	0.38	0.15	0.3	0.60	0.08	-49.91	-35.58	-51.75	107.19	97.89	105.05
Liuzhou	0.89	0.9	0.85	0.79	0.8	0.72	0.74	0.78	0.66	12.71	10.13	11.69	840.36	660.42	748.44
Guilin	0.84	0.79	0.7	0.67	0.59	0.34	0.11	0.34	-0.24	-3.5	-26.89	-17.8	120.08	127.06	142.86
Gongcheng	0.82	0.75	0.71	0.66	0.55	0.21	0.56	0.53	0.15	-2.74	-15.35	10.47	87.81	99.81	95.75
Yangshuo	0.88	0.83	0.62	0.7	0.67	-0.09	0.41	0.56	-0.06	10.82	-7.04	1.99	193.65	174.58	282.08
Pingle	0.88	0.8	0.75	0.72	0.62	0.33	0.57	0.57	0.46	10.87	-6.87	6.02	345.5	360.3	446.48
Wuzhou	0.85	0.94	0.86	0.5	0.84	0.66	0.48	0.57	0.6	3.86	-8.59	0.73	2756.9	2037.8	2208.06
Gaoyao	0.92	0.95	0.88	0.74	0.75	0.66	0.61	0.58	0.68	10.9	2.95	10.09	3024.5	2522.84	2509.4



**Fig. 5.** Scatterplots of simulated and observed monthly streamflow for all stations. The orange and purple lines are the linear regression lines of monthly streamflow for the periods 1980–1984 and 2011–2014, respectively.  $R^2$  is the coefficient of determination. (For interpretation of the references to color in this figure legend, the reader is referred to the web version of this article.)

**Table 4**

Quantitative analysis results of model performance on monthly streamflow simulation.

STATION Time	CC		NSE		NSE (logQ)		Bias (%)		RMSE	
	1980–1984	2011–2014	1980–1984	2011–2014	1980–1984	2011–2014	1980–1984	2011–2014	1980–1984	2011–2014
Maling	0.94	0.96	0.86	0.79	0.61	0.67	-15.04	10.1	20.45	21.4
Gaoche	0.87	0.86	0.75	0.74	0.78	0.7	4.76	-8.97	24.88	21.31
Shihuichang	0.84	0.84	0.59	0.65	0.72	0.69	-23.15	-17.05	88.38	64.57
Huanjiang	0.88	0.72	0.54	0.16	0.7	0.05	-35.62	-51.82	45.36	69.44
Liuzhou	0.96	0.92	0.91	0.83	0.88	0.75	10.13	11.69	294.83	407.89
Guilin	0.93	0.91	0.76	0.78	0.44	0.09	-26.89	-17.76	53.61	50.84
Gongcheng	0.89	0.9	0.76	0.6	0.55	0.33	-15.59	10.65	41.37	44.63
Yangshuo	0.94	0.85	0.85	0.57	0.67	0.35	-7.13	2.06	67.74	118.76
Pingle	0.92	0.94	0.81	0.78	0.7	0.64	-7.06	6.18	152.53	176.99
Wuzhou	0.98	0.93	0.93	0.83	0.63	0.72	-8.62	0.66	1111.09	1451.98
Gaoyao	0.98	0.95	0.87	0.83	0.65	0.81	2.86	10.02	1505.7	1634.48

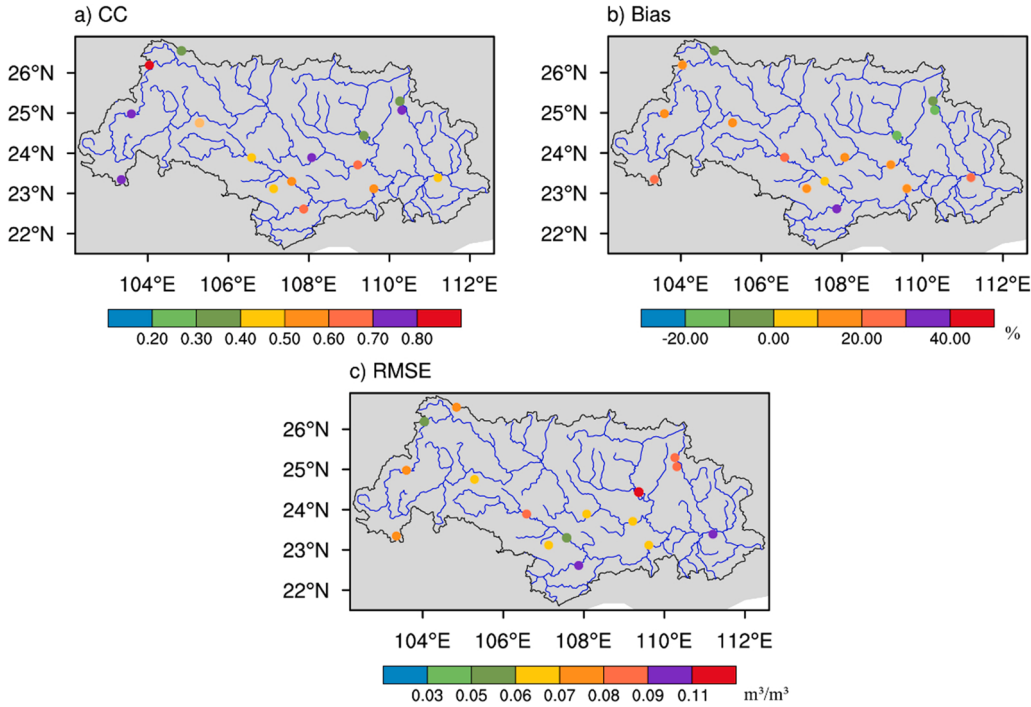


**Fig. 6.** CC (a), Bias (b) and RMSE (c) between simulated monthly soil moisture and station observations during 1992–2013.

Annual average soil moisture and soil temperature (2008–2014) from simulations and CLDAS and the CCs/RMSEs between them are displayed in Fig. 7. Fig. 7(a) and (b) indicate that the model overestimates the soil moisture in the whole basin. And the spatial distributions of simulated and CLDAS soil moisture also demonstrate some differences, especially in the southwest of the basin. CLDAS shows some dry regions located in the southwest of the basin, whereas the model cannot capture this pattern. This is attributed to the soil types used in the model. CLDAS indicates that sandy clay loam is the dominant soil type in the southwest. The soil types used in the model are different (Fig. 3), which makes it hard to reproduce the features specific for sandy clay loam. The spatial pattern of low soil moisture in the west and high soil moisture in the north is reproduced by the model. The CCs between simulations and CLDAS daily soil moisture are larger than 0.75 (Fig. 7(g)), which means that the model can capture the temporal variability of soil moisture. It can be seen from the spatial distribution of RMSEs (Fig. 7(i)) that the biases between the simulations and CLDAS soil moisture are small with the RMSEs lower than  $0.08 \text{ m}^3/\text{m}^3$  in most areas, although the RMSE is higher in some areas of the southwest. In the east area of the basin, the CCs are more than 0.85. The model performance in simulating soil moisture is acceptable with high CCs and low RMSEs. Overall, the model captures the temporal variability of soil moisture, but shows a wetter condition in the first layer, which may be related to the redistribution and re infiltrating processes of the model.

The spatial distributions of annual mean soil temperature (Fig. 7(d) and (e)) from simulations and CLDAS indicate that the simulated soil temperature is a little lower than that of CLDAS. The spatial pattern of the simulated soil temperature is similar to that of the CLDAS soil temperature, and the spatial CC is 0.97. The CLDAS soil temperature is lower in the northwest part of the Xijiang River basin and higher in the southeast. The simulated soil temperature captures this spatial variability. It can be seen from Fig. 7(h) that the CCs are higher than 0.96, which suggests that the model well captures the temporal changes of soil temperature. The RMSEs of soil temperature are smaller than 2 K in most areas, indicating that the model can realistically simulate soil temperature.

Overall, the simulations can capture temporal changes of soil temperature and soil moisture during 2008–2014, and the differences between the simulations and the CLDAS are small. The model performance on the soil temperature simulation is better than the soil moisture simulation.

### 3.1.3. Evapotranspiration

Evapotranspiration (ET) is an important component of the surface water cycle, and it is also an important term in surface energy balance. ET is the sum of soil evaporation (E), plant transpiration (T) and canopy interception, which is closely related to meteorological condition, underlying surface condition and vegetation (Wang et al., 2016). The evapotranspiration products can be roughly divided into two categories: remote sensing retrievals and model simulations (Sun et al., 2013; Zhang et al., 2012).

Fig. 8 shows the CC between the simulated ET and observed daily evaporation during 1980–2017. The evaporation data are downloaded from the China Meteorological Data Network (including 699 basic stations), which includes several stations located in the study region. It can be seen that CCs are lower in the upper part of the basin and higher in the lower part of the basin. The CCs are higher than 0.8 in most areas, and the model can reasonably simulate the variability of ET.

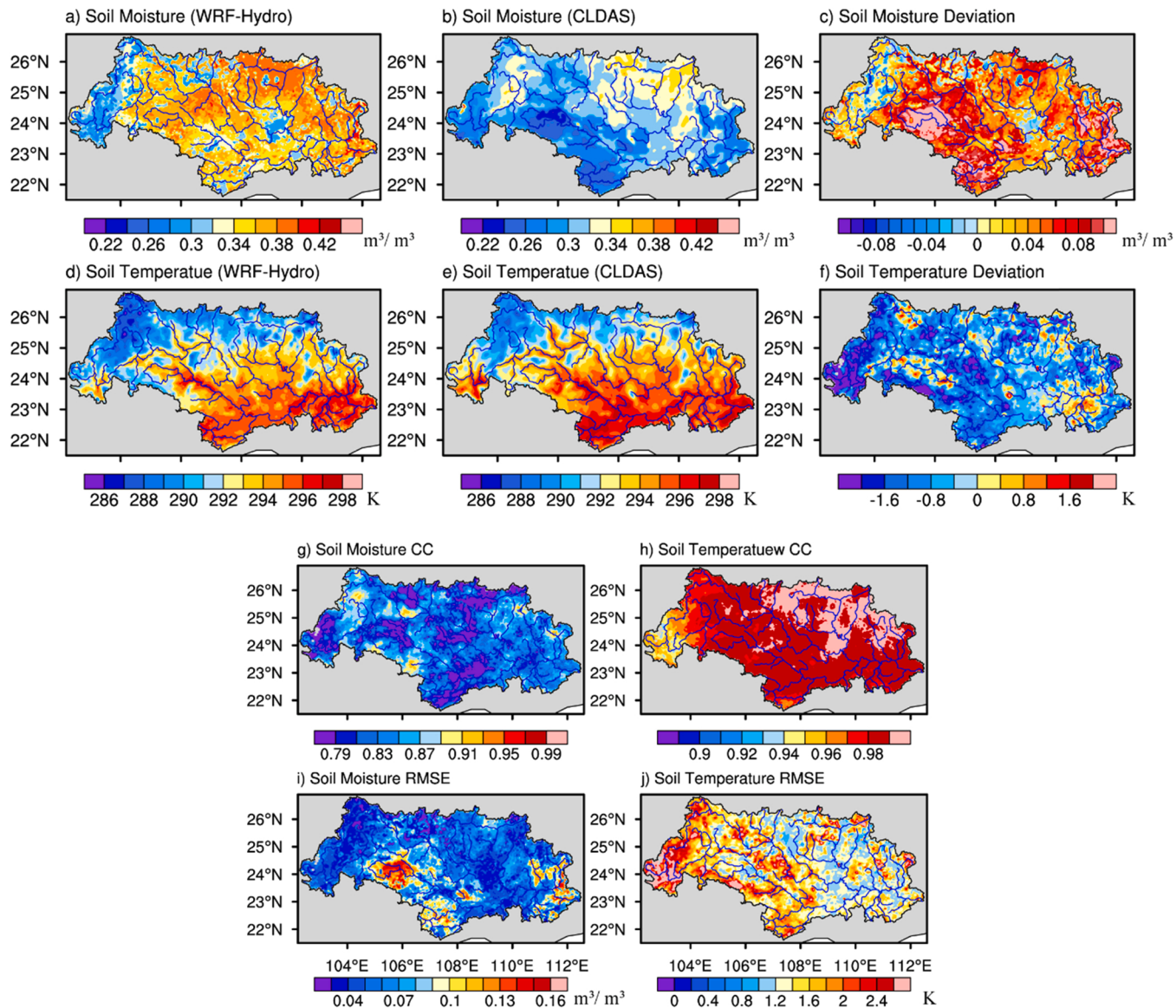


**Fig. 7.** Spatial distributions of annual mean soil moisture and soil temperature from simulations and CLDAS, and the deviations (simulations – CLDAS), CCs and RMSEs between the two datasets for the period 2008–2014.

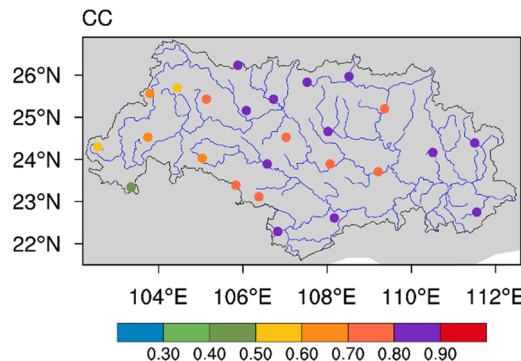


**Fig. 8.** Temporal CCs between simulated daily evapotranspiration and observed daily evaporation (1980–2017).

### 3.2. Streamflow changes

The 5-year running average and linear regression method are employed to reveal the trends of annual streamflow. Fig. 9 shows annual streamflow at 11 stations located in different areas of the basin. From Fig. 9 it can be found that the trends of the streamflow in different areas are spatially uneven. The annual streamflow shows a slightly increasing trend in the downstream of the Xijiang River and a slightly decreasing trend in the upstream. Except for Gongcheng station, there is no significant trend at other stations. The 5-year running average shows that the annual streamflow trends at different stations in the downstream are similar, where a downward trend occurred during 1980–1990 and 1996–2010 while an upward trend appeared during other periods. The changes of the trend at Gaoche and Maling stations are small.

The increasing and decreasing streamflow trends in different seasons are shown in Fig. 10, which indicates that trends in different seasons show different characters. The spring streamflow shows a slightly downward trend at Gaoche, Huangjiang, Gongcheng, Wuzhou and Gaoyao stations and an upward trend in other stations. The summer streamflow shows an upward trend at most stations except Gaoche and Maling stations, where the summer streamflow has a downward trend. The trends of summer streamflow are similar to that of the annual streamflow. Except for Gaoche and Maling stations, the autumn and winter streamflow show an upward trend at all other stations.

The trends of annual 30-day maximum and minimum streamflow are presented in Table 5, which shows that the trends of maximum and minimum streamflow are spatially uneven. The trends in the upstream of the basin change more smoothly than the trends in the downstream. The minimum streamflow at those stations in the Guijiang River and Liujiang River basins displayed a downward trend before 1990 and an upward trend after 1990 (not shown). The annual minimum streamflow demonstrates a continuous downward trend in the upper basin, and an upward trend downstream of the basin. The maximum streamflow changes smoothly at stations in the upstream of the basin, and the maximum streamflow increases significantly at the Guijing River basin. The trends of streamflow of Liujiang and the downstream of Xijiang are similar with an increasing trend before 1995 and a decreasing trend after 1995 (figure not shown). The occurrence dates of the minimum and maximum streamflow change little. The maximum streamflow generally occurs in summer, and the minimum streamflow mostly occurs in winter. Both the low and high pulses increase significantly at most stations. The reversals represent the frequency of streamflow reversing from rising to falling or from falling to rising, and the rise and fall rates stand for the slopes of the rising or falling events, respectively. It can be seen from the table that the reversal and rise rate both increase significantly at most stations, and the fall rate drops distinctly at most stations.

## 4. Discussion

### 4.1. Physical processes

Base flow and lateral processes are two important processes that influence the simulation accuracy, especially for large watersheds. The model uses a simple conceptual bucket base flow model, which connects base flow and overlaying channel in one way. The parameters related to base flow process have no physical meaning. Therefore, these parameters need to be carefully calibrated before using the model. During the calibration, it is found that large basins are more sensitive to these base flow parameters. A better streamflow simulation can be achieved by application of appropriate base flow parameters. The base flow parameters also play an important role in model spin-up, and the values of these parameters in the spin-up period can influence the model performance later. Due to the limitation of the base flow process in the WRF-Hydro, a more physically base flow process could be helpful.

### 4.2. Soil type changes

Soil types can strongly influence the model performance on soil moisture simulation. As each soil type has its unique hydraulic properties, different soil types can lead to different water diversions. In this study, the FAO (Food and Agriculture Organization of the United Nations) soil type dataset (WRF default) used in WRF is replaced by the Beijing Normal University (BNU) soil type dataset (Wei

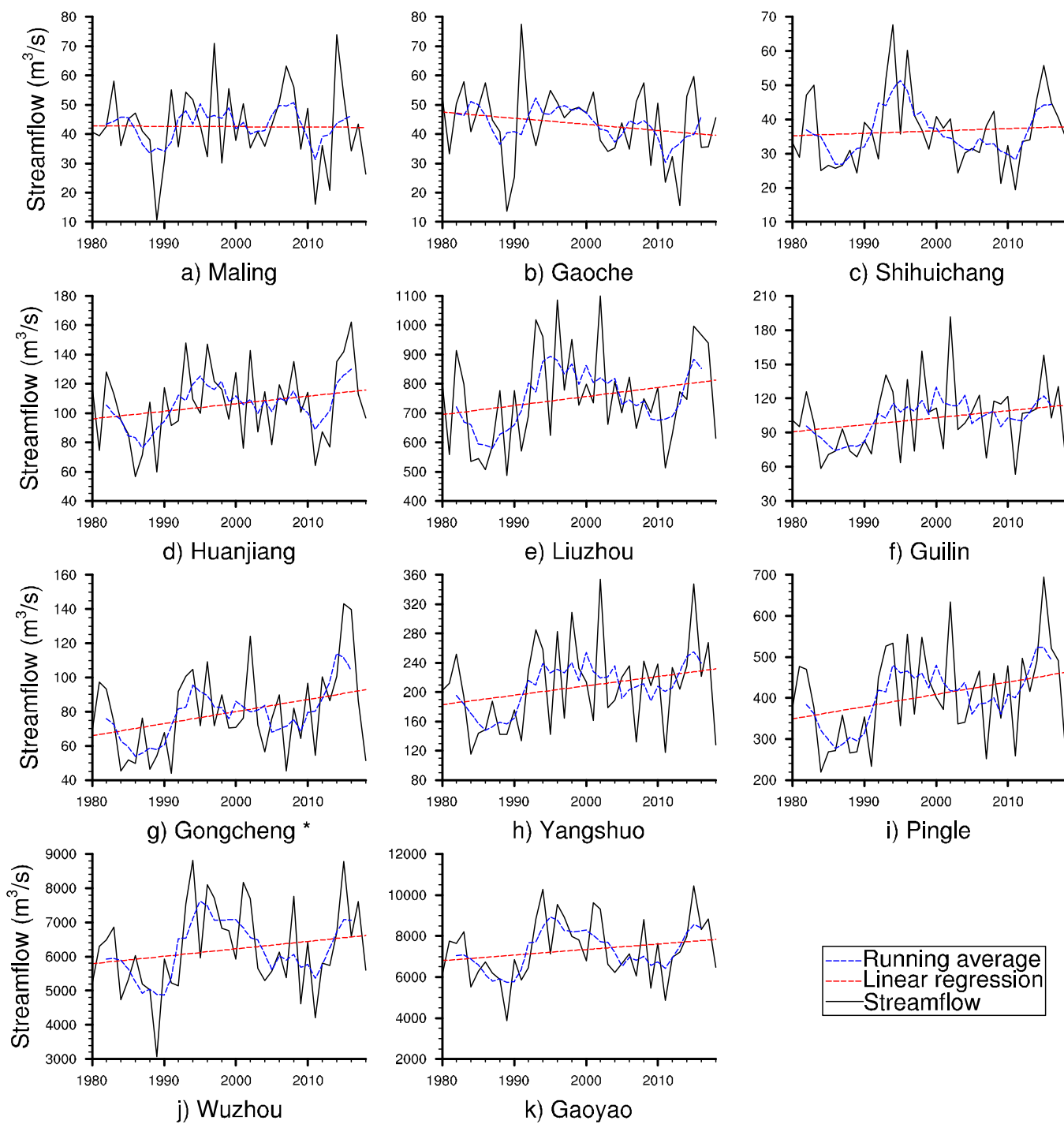
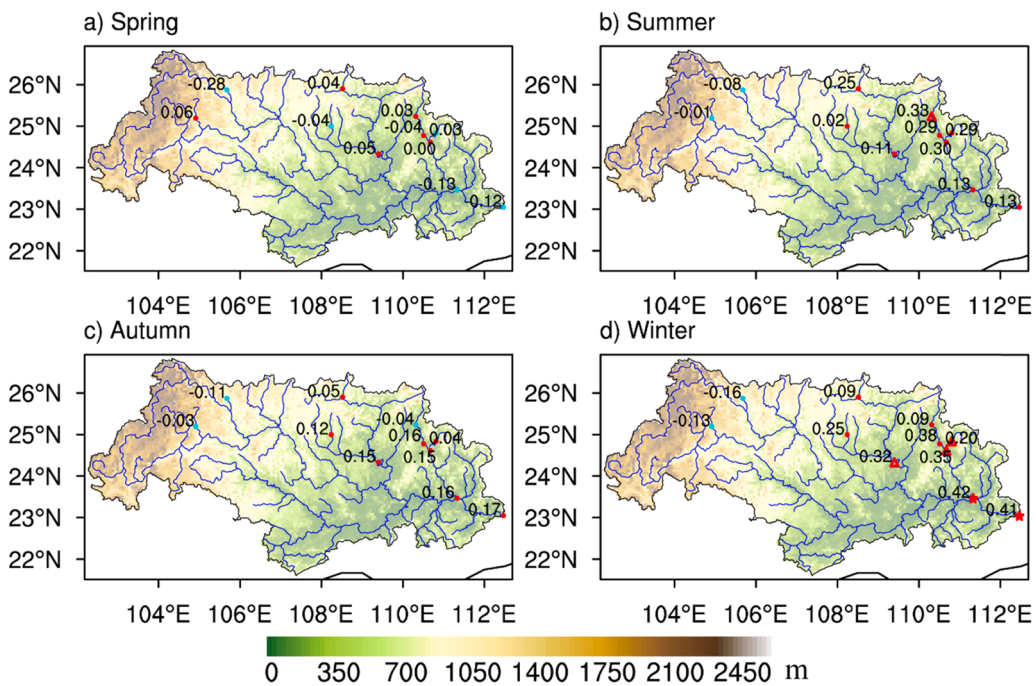


Fig. 9. Trends of yearly streamflow during 1980–2018 at 11 stations, where \* means the trend is significant at the 95% confidence level.



**Fig. 10.** The increasing (red) and decreasing (cyan) trends of seasonal streamflow at all stations. The numbers are the CCs between time and streamflow. Stars and triangles denote trends significant at the 99% and 95% confidence levels, respectively. The background is the DEM (Digital Elevation Model) of the basin. (For interpretation of the references to color in this figure legend, the reader is referred to the web version of this article.)

**Table 5**  
The CCs between time and IHA.

Station	30-day minimum	30-day maximum	Date of minimum	Date of maximum	baseflow	Low pulse	High pulse	Rise rate	Fall rate	reversal
Maling	-0.22	0.03	0.02	0.07	-0.15	0.47**	0.26	0.32*	-0.17	0.54**
Gaoche	-0.25	-0.13	-0.14	-0.06	-0.11	0.53**	0.21	0.04	-0.09	0.74**
Shihuichang	-0.03	0.15	0.03	-0.05	-0.22	0.39*	0.54**	0.55**	-0.43**	0.65**
Huangjiang	0.08	-0.04	-0.21	-0.03	0.01	0.48**	0.36*	0.31	-0.21	0.39*
Liuzhou	0.22	0.01	0.13	-0.20	0.00	0.41**	0.51**	0.36*	-0.35*	0.85**
Guilin	-0.22	0.27	0.17	-0.11	-0.36*	0.41**	0.23	0.45**	-0.02	0.68**
Gongchen	0.20	0.35*	0.19	0.08	-0.17	0.07	0.56**	0.49**	-0.32*	0.65**
Yangshuo	0.01	0.32*	0.26	-0.06	-0.34*	0.17	0.34*	0.44**	-0.31	0.67**
Pingle	0.22	0.32*	0.21	-0.18	-0.21	0.12	0.30	0.51**	-0.39*	0.74**
Wuzhou	0.39*	0.06	0.10	-0.04	0.28	0.28	0.35*	0.49**	-0.38*	0.76**
Gaoyao	0.47**	0.08	0.00	0.06	0.31	0.36*	0.44**	0.52**	-0.37*	0.77**

\* Means the CC is significant at the 95% confidence level test, \*\* means the CC is significant at the 99% confidence level.

et al., 2014). The FAO soil type dataset used in WRF was produced by the U.S. Department of Agriculture in 1991, which includes 12 basic types determined according to the content of each soil type component. The spatial resolution of this dataset can reach 30" in the United States, but the dataset uses 5' data provided by FAO in other regions. In China, this dataset is produced using the 1:5 million soil distribution map and 60 soil profiles data in the World Emissions Inventory project, and these 60 profiles are mainly located in northern China. Therefore, the correctness and accuracy of this dataset are questionable in China. The BNU soil type dataset is produced based on the 1:1 million soil distribution map of China and contains nearly 9000 original soil profiles, therefore, it can represent the soil spatial heterogeneity better than the FAO dataset, especially in regions outside of northern China (such as, southern China). Strict quality control is conducted during the integration of the profile dataset, and the type connection method and distance connection method are adopted to develop the final Chinese soil attribute dataset (Wei et al., 2014). The spatial distributions of soil types from different datasets in Xijiang River basin are displayed in Fig. 11, which shows that the difference between these two datasets is large. The soil type in the west part of the basin is clay in the FAO dataset, but it is clay loam in the BNU dataset. In the southwest area, the soil type changes from sandy clay loam in the FAO dataset to clay loam in the BNU dataset. In the northeast part, the soil type changes from clay loam in the default to silty clay in the BNU dataset. And in the southeast area, it changes from sandy clay loam to clay. The changes of soil types can influence the model simulation of soil moisture.

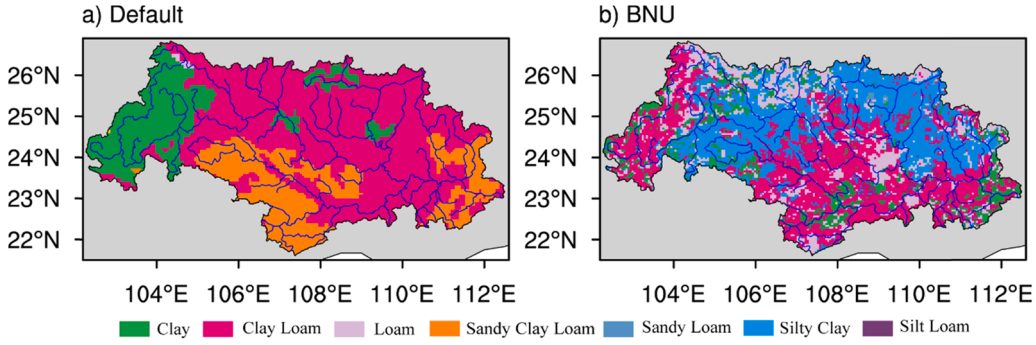


Fig. 11. Spatial distributions of soil type: a) the FAO dataset, b) the BNU dataset.

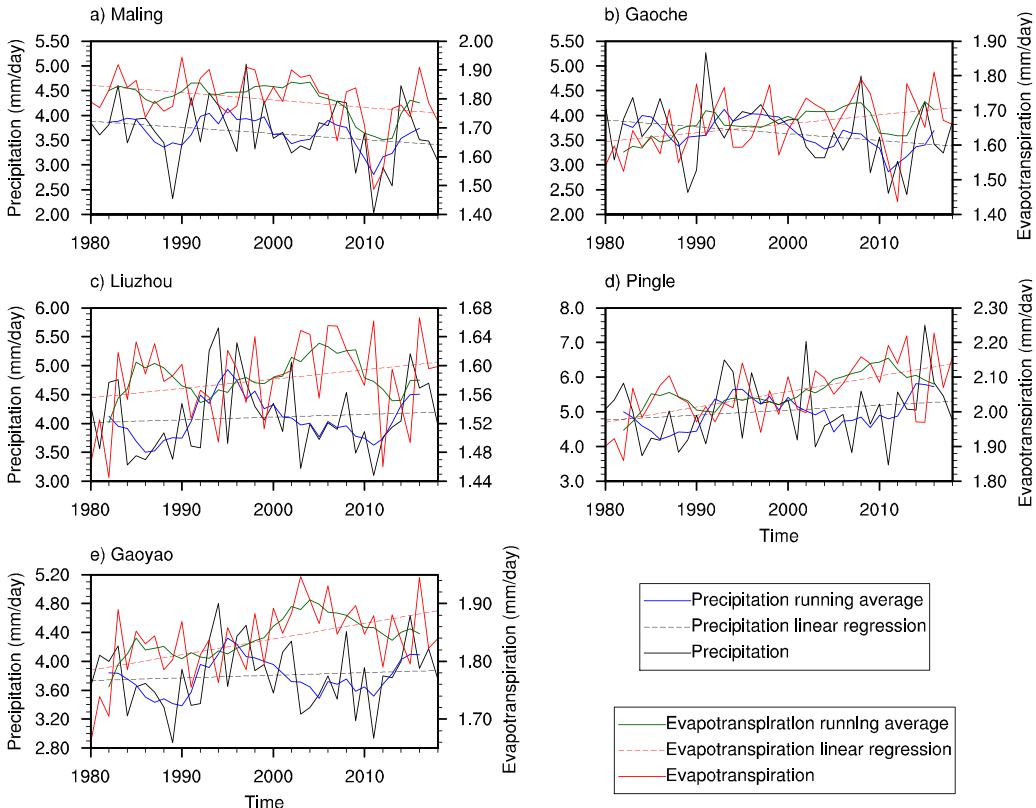


Fig. 12. Trends of annual precipitation and evapotranspiration in five basins during 1980–2018.

#### 4.3. The possible reason for streamflow change

It can be seen from Section 3.2 that the trends of streamflow are different in different areas of the basin. In this section, the reasons are roughly discussed based on precipitation and evapotranspiration (ET). The trends of annual precipitation and ET are similar in the basin where the Maling station is located, and their trends may lead to the trend of streamflow at Maling station. The same results can be found at Gaoche station. The running averages of precipitation and ET shown in Fig. 12(c) indicate that the trends of precipitation and ET are in opposite direction, that is, precipitation increase while ET decrease. The trend of streamflow is similar to the trend of precipitation, and the opposite trends of precipitation and ET mentioned above could strengthen the trend of streamflow. The same results can be found in Fig. 12(d) and (e). The changes of streamflow may be the results of changes in precipitation and ET.

## 5. Conclusions

There are different topographies and land use types in the Xijiang River basin such as mountains and plains, crop lands and forests,

etc. Simulation and forecast of streamflow in this basin are challenging. In the present study, a relatively new and comprehensive distributed hydrological model—WRF-Hydro is evaluated for its ability to simulate hydrological conditions in the whole basin. WRF-Hydro is coupled with the Noah LSM, which describes complete kinetic and thermal processes. Traditional metrics of CC, NSE,  $NSE(\log Q)$ , RMSE and Bias statistical indices are used to evaluate the performance of the distributed WRF-Hydro hydrological model in the Xijiang River basin and its several sub-basins. The periods of 1980–1984 and 2006–2014 are chosen for the present study. The period of 2006–2010 is used for calibration and the periods of 1980–1984 and 2011–2014 are used for verification.

The results show that the performance of the model is acceptable for both the calibration period and the two verification periods. The CC of the simulated daily streamflow is above 0.5 for almost all the stations, and it reaches 0.8 for some stations. This result indicates that the model can reasonably simulate the temporal variation of daily streamflow. The NSE is relatively high and can reach 0.76 for some stations, suggesting that the model performance in simulating daily streamflow is acceptable in this basin. Based on the hydrographs and the results of the statistical metrics, it can be concluded that this model has the ability to capture the peak streamflow and the minimum streamflow in the recession periods. The CC of monthly streamflow is larger than 0.9, which means that this model can well simulate the seasonal variations of the streamflow. The model performance on simulating monthly streamflow can be regarded as ‘good’ for most stations and ‘very good’ for some stations.

The model also has the ability to simulate hydrological variables such as evapotranspiration, soil temperature and soil moisture, etc. From the statistical metrics, it can be seen that the model can properly simulate the temporal variations of soil moisture and soil temperature. The performance on simulating soil temperature is better than that of soil moisture. The CCs between simulated evapotranspiration and observed evaporation are high, which implies that this model has the ability to simulate the temporal variations of evapotranspiration.

The trends of annual and seasonal streamflow are spatially uneven in the Xijiang River basin, both of which decrease in the upper part and increase in the lower part. Some statistical metrics (such as the reversals) also show significant increasing/decreasing trends.

The present study indicates that the model can be used not only in small watersheds but also in large watersheds, and its performance in simulating streamflow in different areas of a watershed is acceptable. Besides, the model can be used in basins with various terrains (such as mountains and plains) and different land use types.

In summary, the offline WRF-Hydro model is a useful tool to simulate streamflow and hydrological conditions of both large and small watersheds in the Xijiang River basin. It can be used for practical research such as the simulation and prediction of hydrological variability in this basin. However, the model applications in real-time forecast and seasonal prediction still need to be evaluated in South China. Also, its performances in other main river basins of China such as the Yangtze River and the Yellow River basins, and its simulation abilities in different climate zones such as the semi-arid and arid zones still need to be examined.

#### CRediT authorship contribution statement

**Songnan Liu:** Methodology, Software, Formal analysis, Visualization, Writing – original draft. **Jun Wang:** Conceptualization, Methodology, Writing – review & editing. **Jiangfeng Wei:** Writing – review & editing. **Huijun Wang:** Conceptualization, Writing – review & editing, Funding acquisition.

#### Declaration of Competing Interest

The authors declare that they have no known competing financial interests or personal relationships that could have appeared to influence the work reported in this paper.

#### Acknowledgments

We appreciate the team of Prof. Kun Yang in Tsinghua University to provide the China Meteorological Forcing Dataset and the team of Prof. Chunxiang Shi in National Meteorological Information Center to provide the Global Land Data Assimilation System Dataset. This paper is Supported by the National Natural Science Foundation of China (Grant No. 42088101 and No. 41991283).

#### Appendix A. Supporting information

Supplementary data associated with this article can be found in the online version at [doi:10.1016/j.ejrh.2021.100943](https://doi.org/10.1016/j.ejrh.2021.100943). These data include Google maps of the most important areas described in this article.

#### References

- Arnault, J., Wagner, S., Rummel, T., Fersch, B., Bliefernicht, J., Andresen, S., Kunstmann, H., 2016. Role of runoff–infiltration partitioning and resolved overland flow on land-atmosphere feedbacks: a case study with the WRF-Hydro coupled modeling system for West Africa. *J. Hydrometeorol.* 17, 1489–1516. <https://doi.org/10.1175/JHM-D-15-0089.1>.
- Bai, Y.Y., Scott, T.A., Chen, W.P., Chang, A.C., 2010. Evaluating methods for measuring the mean soil temperature. *Geoderma* 157, 222–227. <https://doi.org/10.1016/j.geoderma.2010.04.021>.

- Beskow, S., Mello, C.R., Norton, L.D., da Silva, A.M., 2011. Performance of a distributed semi-conceptual hydrological model under tropical watershed conditions. *Catena* 86, 160–171. <https://doi.org/10.1016/j.catena.2011.03.010>.
- Carson, J.E., Moses, H., 1963. The annual and diurnal heat-exchange cycles in upper layers of soil. *J. Appl. Meteorol.* 2, 397–406. [https://doi.org/10.1175/1520-0450\(1963\)002<0397:taadhe>2.0.co;2](https://doi.org/10.1175/1520-0450(1963)002<0397:taadhe>2.0.co;2).
- Chen, T., Ren, L., Yuan, F., Tang, T., Yang, X., Jiang, S., Liu, Y., Zhao, C., Zhang, L., 2019. Merging ground and satellite-based precipitation data sets for improved hydrological simulations in the Xijiang River basin of China. *Stoch. Environ. Res. Risk Assess.* 33, 1893–1905.
- Chen, Y.Y., Yang, K., He, J., Qin, J., Shi, J.C., Du, J.Y., He, Q., 2011. Improving land surface temperature modeling for dry land of China. *J. Geophys. Res. Atmos.* 116, 1–15. <https://doi.org/10.1029/2011JD015921>.
- Cui, W.Z., Chen, J., Wu, Y.P., Wu, Y.D., 2007. An overview of water resources management of the Pearl River. *Water Sci. Technol. Water Supply* 7, 101–113. <https://doi.org/10.2166/ws.2007.045>.
- Devia, G.K., Ganasri, B.P., Dwarakish, G.S., 2015. A review on hydrological models. *Aquat. Procedia* 4, 1001–1007. <https://doi.org/10.1016/j.aqpro.2015.02.126>.
- Douville, H., Chauvin, F., 2000. Relevance of soil moisture for seasonal climate predictions: a preliminary study. *Clim. Dyn.* 16, 719–736. <https://doi.org/10.1007/s003820000080>.
- Gochis, D.J., Barlage, M., Dugger, A., Fitzgerald, K., Karsten, L., McAllister, M., McCreight, J., Mills, J., Rafieeinasab, A., Read, L., Sampson, K., Yates, D., Yu, W., 2018. WRF-Hydro V5 Technical Description. NCAR Technical Note. Center for Atmospheric Research (NCAR), Boulder, CO, USA.
- Guo, Z.C., Dirmeyer, P.A., 2006. Evaluation of the Second Global Soil Wetness Project soil moisture simulations: 1. Intermodel comparison. *J. Geophys. Res. Atmos.* 111, 1–14. <https://doi.org/10.1029/2006JD007233>.
- Han, S., Shi, C.X., Lin, H.J., Meng, X.Y., Lu, H.Q., 2015. The CLDAS soil moisture operation products applied to monitor soil drought (in Chinese). *J. Glaciol. Geocryol.* 37, 446–453.
- Hersbach, H., Bell, B., Berrisford, P., Hirahara, S., Horányi, A., Muñoz-Sabater, J., Nicolas, J., Peubey, C., Radu, R., Schepers, D., Simmons, A., Soci, C., Abdalla, S., Abellán, X., Balsamo, G., Bechtold, P., Biavati, G., Bidlot, J., Bonavita, M., De Chiara, G., Dahlgren, P., Dee, D., Diamantakis, M., Dragani, R., Flemming, J., Forbes, R., Fuentes, M., Geer, A., Haimberger, L., Healy, S., Hogan, R.J., Hölm, E., Janisková, M., Keeley, S., Laloyaux, P., Lopez, P., Lupu, C., Radnoti, G., de Rosnay, P., Rozum, I., Vamborg, F., Villaume, S., Thépaut, J.N., 2020. The ERA5 global reanalysis. *Q. J. Roy. Meteor. Soc.* 146, 1999–2049. <https://doi.org/10.1002/qj.3803>.
- Jiang, H., Chen, J., Guan, Q., Dong, L., Fu, C., 2011. Comparison of monthly runoff for different scaling basin and sensitivity analysis: a case study in the Xijiang Watershed (in Chinese). *J. Subtrop. Resour. Environ.* 6 (01), 45–55.
- Kerandji, N., Arnault, J., Laux, P., Wagner, S., Kitheka, J., Kunstmann, H., 2017. Joint atmospheric-terrestrial water balances for East Africa: a WRF-Hydro case study for the upper Tana River basin. *Theor. Appl. Climatol.* 131, 1337–1355. <https://doi.org/10.1007/s00704-017-2050-8>.
- Legates, D.R., Mahmood, R., Levina, D.F., DeLiberty, T.L., Quiring, S.M., Houser, C., Nelson, F.E., 2011. Soil moisture: a central and unifying theme in physical geography. *Prog. Phys. Geogr.* 35, 65–86. <https://doi.org/10.1177/0309133310386514>.
- Lechner, B., Verdin, K., Jarvis, A., 2008. New global hydrography derived from spaceborne elevation data. *EOS, Trans. Am. Geophys. UNION* 89, 93–94. <https://doi.org/10.1029/2008EO100001>.
- Lei, X.H., Liao, W.H., Wang, Y.H., Jiang, Y.Z., Wang, H., Tian, Y., 2014. Development and application of a distributed hydrological model: EasyDHM. *J. Hydrol. Eng.* 19, 44–59. [https://doi.org/10.1061/\(ASCE\)HE.1943-5584.0000745](https://doi.org/10.1061/(ASCE)HE.1943-5584.0000745).
- Lin, P.R., Yang, Z.L., Gochis, D.J., Yu, W., Maidment, D.R., Somos-Valenzuela, M.A., David, C.H., 2018. Implementation of a vector-based river network routing scheme in the community WRF-Hydro modeling framework for flood discharge simulation. *Environ. Model. Softw.* 107, 1–11. <https://doi.org/10.1016/j.envsoft.2018.05.018>.
- Lin, Q.X., Wu, Z.Y., Singh, V.P., Sadeghi, S.H.R., He, H., Lu, G.H., 2017. Correlation between hydrological drought, climatic factors, reservoir operation, and vegetation cover in the Xijiang Basin, South China. *J. Hydrol.* 549, 512–524. <https://doi.org/10.1016/j.jhydrol.2017.04.020>.
- Liu, C.M., Wang, Z.G., Zheng, H.X., Zhang, L., Wu, X.F., 2008. Development of hydro-informatic modelling system and its application. *Sci. China, Ser. E Technol. Sci.* 51, 456–466. <https://doi.org/10.1007/s11431-008-0040-x>.
- Liu, X.M., Yang, T.T., Hsu, K.L., Liu, C.M., Sorooshian, S., 2017. Evaluating the streamflow simulation capability of PERSIANN-CDR daily rainfall products in two river basins on the Tibetan Plateau. *Hydrol. Earth Syst. Sci.* 21, 169–181. <https://doi.org/10.5194/hess-21-169-2017>.
- Ma, N., Szilagyi, J., Zhang, Y.S., Liu, W.B., 2019. Complementary-relationship-based modeling of terrestrial evapotranspiration across China during 1982–2012: validations and spatiotemporal analyses. *J. Geophys. Res. Atmos.* 124, 4326–4351. <https://doi.org/10.1029/2018JD029850>.
- Moriasi, D.N., Arnold, J.G., Van Liew, M.W., Bingner, R.L., Harmel, R.D., Veith, T.L., 2007. Model evaluation guidelines for systematic quantification of accuracy in watershed simulations. *Trans. ASABE* 50, 885–900.
- Motovilov, Y.G., Gottschalk, L., Engeland, K., Rodhe, A., 1999. Validation of a distributed hydrological model against spatial observations. *Agric. For. Meteorol.* 98–99, 257–277. [https://doi.org/10.1016/S0168-1923\(99\)00102-1](https://doi.org/10.1016/S0168-1923(99)00102-1).
- Naabil, E., Lampert, B.L., Arnault, J., Olufayo, A., Kunstmann, H., 2017. Water resources management using the WRF-Hydro modelling system: case-study of the Tono dam in West Africa. *J. Hydrol. Reg. Stud.* 12, 196–209.
- Nash, J.E., Sutcliffe, J.V., 1970. River flow forecasting through conceptual models part I – a discussion of principles. *J. Hydrol.* 10, 282–290. [https://doi.org/10.1016/0022-1694\(70\)90255-6](https://doi.org/10.1016/0022-1694(70)90255-6).
- Niu, J., Chen, J., Sun, L.Q., 2015. Exploration of drought evolution using numerical simulations over the Xijiang (West River) basin in South China. *J. Hydrol.* 526, 68–77. <https://doi.org/10.1016/j.jhydrol.2014.11.029>.
- Rummel, T., Arnault, J., Gochis, D., Kunstmann, H., 2019. Role of lateral terrestrial water flow on the regional water cycle in a complex terrain region: investigation with a fully coupled model system. *J. Geophys. Res. Atmos.* 124, 507–529. <https://doi.org/10.1029/2018JD029004>.
- Ryu, Y., Lim, Y.J., Ji, H.S., Park, H.H., Chang, E.C., Kim, B.J., 2017. Applying a coupled hydrometeorological simulation system to flash flood forecasting over the Korean Peninsula. *Asia-Pac. J. Atmos. Sci.* 53, 421–430. <https://doi.org/10.1007/s13143-017-004+5-0>.
- Senatore, A., Mendicino, G., Gochis, D.J., Yu, W., Yates, D.N., Kunstmann, Harald, 2015. Fully coupled atmosphere-hydrology simulations for the central Mediterranean: impact of enhanced hydrological parameterization for short and long time scales. *J. Adv. Model. Earth Syst.* 7, 1693–1715. <https://doi.org/10.1002/2013MS000282>. Received.
- Shan, H., Yuan, F., Sheng, D., Sun, F., 2015. The application of VIC model to runoff simulation of Xijiang River basin (in Chinese). *China Rural Water Hydropower* 4, 43–45.
- Silver, M., Karniel, A., Ginat, H., Meiri, E., Fredj, E., 2017. An innovative method for determining hydrological calibration parameters for the WRF-Hydro model in arid regions. *Environ. Modell. Softw.* 91, 47–69.
- Skamarock, W.C., Klemp, J.B., Dudhia, J., Gill, D.O., Barker, D.M., Duda, M.G., Huang, X.-Y., Wang, W., Powers, J.G., 2008. A Description of the Advanced Research WRF Version 3. Center for Atmospheric Research (NCAR), Boulder, CO, USA.
- Somos-Valenzuela, A.M., Palmer, N.R., 2018. Use of WRF-Hydro over the Northeast of the US to estimate water budget tendencies in small watersheds. *Water* 10, 1709–1725. <https://doi.org/10.3390/w10121709>.
- Stéfanon, M., Drobinski, P., D'Andrea, F., Lebeaupin-Brossier, C., Bastin, S., 2013. Soil moisture-temperature feedbacks at meso-scale during summer heat waves over Western Europe. *Clim. Dyn.* 42, 1309–1324. <https://doi.org/10.1007/s00382-013-1794-9>.
- Sun, F.F., Xu, Q., Ren, L.L., Shan, H.C., Kong, H., 2013. Evapotranspiration calculation and runoff simulation in the context of BTOPMC model (in Chinese). *China Rural Water Hydropower* 12, 85–88.
- Sun, S.B., Chen, B.Z., Shao, Q.Q., Chen, J., Liu, J.Y., Zhang, X.J., Zhang, H.F., Lin, X.F., 2017. Modeling evapotranspiration over China's landmass from 1979 to 2012 using multiple land surface models: evaluations and analyses. *J. Hydrometeorol.* 18, 1125–1180. <https://doi.org/10.1175/JHM-D-16-0212.1>.
- Sun, Y.Q., Niu, J., 2019. Regionalization of daily soil moisture dynamics using wavelet-based multiscale entropy and principal component analysis. *Entropy* 21, 548–559. <https://doi.org/10.3390/e21060548>.
- Tedeschi, L.O., 2006. Assessment of the adequacy of mathematical models. *Agric. Syst.* 89, 225–247. <https://doi.org/10.1016/j.agryea.2005.11.004>.

- Tuttle, S., Salvucci, G., 2016. Atmospheric science: empirical evidence of contrasting soil moisture-precipitation feedbacks across the United States. *Science* 352, 825–828. <https://doi.org/10.1126/science.aaa7185>.
- Varlas, G., Katsafados, P., Papadopoulos, A., Korres, G., 2018. Implementation of a two-way coupled atmosphere-ocean wave modeling system for assessing air-sea interaction over the Mediterranean Sea. *Atmos. Res.* 208, 201–217. <https://doi.org/10.1016/j.atmosres.2017.08.019>.
- Varlas, G., Anagnostou, M.N., Spyrou, C., Papadopoulos, A., Kalogiros, J., Mentzafou, A., Michaelides, S., Baltas, E., Karymbalis, E., Katsafados, P., 2019. A multi-platform hydrometeorological analysis of the flash flood event of 15 November 2017 in Attica, Greece. *Remote Sens.* 11, 45–75. <https://doi.org/10.3390/rs11010045>.
- Walker, J., Rowntree, P.R., 1977. The effect of soil moisture on circulation and rainfall in a tropical model. *Q. J. R. Meteorol. Soc.* 103, 29–46. <https://doi.org/10.1002/qj.49710343503>.
- Wang, J., Wang, H.J., Hong, Y., 2016. A high-resolution flood forecasting and monitoring system for China using satellite remote sensing data (in Chinese). *Chinese Sci. Bull.* 61, 518–528. <https://doi.org/10.1360/N972015-00489>.
- Wang, J.H., Hong, Y., Li, L., Gourley, J.J., Sadiq, K.I., Yilmaz, K.K., Adler, R.F., Policelli, F.S., Habib, S., Irwn, D., Limaye, A.S., Korme, T., Okello, L., 2011. The coupled routing and excess storage (CREST) distributed hydrological model. *Hydrol. Sci. J.* 56, 84–98. <https://doi.org/10.1080/02626667.2010.543087>.
- Wei, J.F., Dickinson, R.E., Chen, H.S., 2008. A negative soil moisture-precipitation relationship and its causes. *J. Hydrometeorol.* 9, 1364–1376.
- Wei, J.F., Dirmeyer, P.A., 2012. Dissecting soil moisture-precipitation coupling. *Geophys. Res. Lett.* 39, L19711 <https://doi.org/10.1029/2012GL053038>.
- Wei, S.G., Dai, Y.J., Duan, Q.Y., Liu, B.Y., Hua, Y., 2014. A global soil data set for earth system modeling. *J. Adv. Model. Earth Syst.* 6 (1), 249–263.
- Winsemius, H.C., Aerts, J.C.J.H., Van Beek, L.P.H., Bierkens, M.F.P., Bouwman, A., Jongman, B., Kwadijk, J.C.J., Ligvoet, W., Lucas, P.L., Van Vuuren, D.P., Ward, P.J., 2016. Global drivers of future river flood risk. *Nat. Clim. Chang.* 6, 381–385. <https://doi.org/10.1038/nclimate2893>.
- Wu, J., Gao, X.J., 2013. A gridded daily observation dataset over China region and comparison with the other datasets (in chinese). *Chinese J. Geophys.* 56, 1102–1111.
- Xue, Y.K., Vasic, R., Janjic, Z., Liu, Y.M., Chu, P.C., 2012. The impact of spring subsurface soil temperature anomaly in the western U.S. on North American summer precipitation: a case study using regional climate model downscaling. *J. Geophys. Res. Atmos.* 117, 1–11. <https://doi.org/10.1029/2012JD017692>.
- Yu, S., He, S.Y., Sun, P.A., Pu, J.B., Huang, J., Luo, H.X., Li, Y.S., Li, R., Yuan, Y.Q., 2016. Impacts of anthropogenic activities on weathering and carbon fluxes: a case study in the Xijiang River basin, southwest China. *Environ. Earth Sci.* 75, 589–599. <https://doi.org/10.1007/s12665-015-5226-5>.
- Yuan, F., Zhao, C.X., Jiang, Y., Ren, L.L., Shan, H.C., Zhang, L.M., Zhu, Y.H., 2017. Evaluation on uncertainty sources in projecting hydrological changes over the Xijiang River basin in South China. *J. Hydrol.* 554, 434–450. <https://doi.org/10.1016/j.jhydrol.2017.08.034>.
- Yuan, Y., Lei, X., Jiang, Y., Song, W., 2014. Research on Hydrological Simulation in Xijiang Basin Based on SWAT Model (in Chinese). *China Rural Water Hydropower* 3, 14–17.
- Yucel, I., Onen, A., Yilmaz, K.K., Gochis, D.J., 2015. Calibration and evaluation of a flood forecasting system: Utility of numerical weather prediction model, data assimilation and satellite-based rainfall. *J. Hydrol.* 523, 49–66. <https://doi.org/10.1016/j.jhydrol.2015.01.042>.
- Zhang, Q., Xu, C.Y., Zhang, Z.X., 2009. Observed changes of drought/wetness episodes in the Pearl River basin, China, using the standardized precipitation index and aridity index. *Theor. Appl. Climatol.* 98, 89–99. <https://doi.org/10.1007/s00704-008-0095-4>.
- Zhang, R.H., Du, J.P., Sun, R., 2012. Review of estimation and validation of regional evapotranspiration based on remote sensing (in Chinese). *Adv. Earth Sci.* 27, 1295–1307. [https://doi.org/10.1016/0016-0032\(66\)90270-5](https://doi.org/10.1016/0016-0032(66)90270-5).
- Zhong, J., Li, S.L., Liu, J., Ding, H., Sun, X.Le, Xu, S., Wang, T.J., Ellam, R.M., Liu, C.Q., 2018. Climate variability controls on CO<sub>2</sub> consumption fluxes and carbon dynamics for monsoonal rivers: evidence from Xijiang River, Southwest China. *J. Geophys. Res. Biogeosci.* 123, 2553–2567. <https://doi.org/10.1029/2018JG004439>.